Evidence for momentum-dependent heavy-fermionic electronic structures: Soft x-ray ARPES for the superconductor $CeNi_2Ge_2$ in the normal state

Y. Nakatani,[1] H. Aratani,[1] H. Fujiwara,[1] T. Mori,[1] A. Tsuruta,[1] S. Tachibana,[1] T. Yamaguchi,[1] T. Kiss,[1] A. Yamasaki,[2] A. Yasui,[3,4] H. Yamagami,[3,5] J. Miyawaki,[6] T. Ebihara,[7] Y. Saitoh,[3] and A. Sekiyama[1]

[1]*Division of Materials Physics, Graduate School of Engineering Science, Osaka University, Toyonaka, Osaka 560-8531, Japan*

[2]*Faculty of Science and Engineering, Konan University, Kobe 658-8501, Japan*

[3]*Materials Sciences Research Center, Japan Atomic Energy Agency, Sayo, Hyogo 679-5148, Japan*

[4]*Japan Synchrotron Radiation Research Institute, Sayo, Hyogo 679-5198, Japan*

[5]*Faculty of Science, Kyoto Sangyo University, Kyoto 603-8047, Japan*

[6]*The Institute for Solid State Physics, The University of Tokyo, Kashiwa, Chiba 277-8581, Japan*

[7]*Department of Physics, Shizuoka University, Shizuoka 422-8529, Japan*

(Received 7 July 2017; revised manuscript received 17 January 2018; published 29 March 2018)

We present clear experimental evidence for the momentum-dependent heavy fermionic electronic structures of the $4f$-based strongly correlated system $CeNi_2Ge_2$ by soft x-ray angle-resolved photoemission spectroscopy. A comparison between the experimental three-dimensional quasiparticle dispersion of $LaNi_2Ge_2$ and $CeNi_2Ge_2$ has revealed that heavy fermionic electronic structures are seen in the region surrounding a specific momentum. Furthermore, the wave vectors between the observed "heavy spots" are consistent with a result of neutron scattering reflecting magnetic correlations, which could be a trigger for the superconductivity in $CeNi_2Ge_2$.

DOI: 10.1103/PhysRevB.97.115160

I. INTRODUCTION

The physics of strongly correlated $4f$-based heavy fermion (HF) systems is a long-standing challenge, where many fascinating phenomena are seen in the vicinity of the quantum critical point (QCP), such as an enormous effective mass enhancement [1–6], unconventional superconducting transitions [2,5], and a competition or cooperation between magnetism and superconductivity [6–10]. HF behavior arising from the hybridization between the mobile non-$4f$ and localized $4f$ orbitals (cf hybridization) is macroscopically observed through the Sommerfeld coefficient γ, which is in proportion to the Fermi-surface-averaged effective mass. Microscopically, the effective mass m^* at the Fermi level (E_F) can be probed by angle-resolved photoemission spectroscopy (ARPES) through the band/quasiparticle dispersion as

$$v_F = \hbar^{-1}|dE/dk|_{k=k_F}, \quad (1)$$

$$m^* = \hbar k_F / v_F, \quad (2)$$

where v_F, E, $\hbar k$, and $\hbar k_F$ denote the Fermi velocity, binding energy, momentum, and Fermi momentum, respectively. Since ARPES is advantageous to investigate momentum-dependent electronic structures compared to other probes, such as quantum oscillation experiments, intensive studies have been performed to reveal the quasiparticle band structures in HF materials [11–24].

Nevertheless, only a few ARPES works have been reported for the renormalized (heavy) bands of HF systems [12,13,21]. The lack of microscopic experimental information makes it difficult to reveal the origin of the quantum criticality for realistic HF systems, which is proposed on the basis of several models due to the spin fluctuation [25], Kondo breakdown [26–28], and valence fluctuation theories [29,30]. The HF phenomena are complicated by the strong momentum dependence of a HF nature arising from anisotropic cf hybridizations, which reflect the $4f$ charge distributions as clearly revealed by soft x-ray absorption spectroscopy [31–33]. To tackle this problem, it is essential to seriously investigate the band structures along various directions in three-dimensional (3D) reciprocal space.

A family of Ce-based ternary compounds with a tetragonal $ThCr_2Si_2$ structure is a benchmark system for the study of such anisotropic electronic states with a rich variety of the ground-state properties mentioned above. Here, we focus on $CeNi_2Ge_2$, which shows non-Fermi-liquid behavior with a superconducting phase transition at an ambient pressure below 0.2 K [5], suggesting that the ground states are close to QCP. γ is evaluated as 350 mJ/(mol K^2) [3], which is comparable to that of a typical HF material $CeRu_2Si_2$ [4]. The satellite structures appearing in the Ce $3d$ x-ray absorption [34–37] spectrum demonstrate a sizable cf hybridization in $CeNi_2Ge_2$ [38].

In this paper, we present direct evidence for the formation of momentum-dependent HF bands in $CeNi_2Ge_2$ by using soft x-ray ARPES, which is a suitable probe to select the momentum not only within the k_x-k_y plane parallel to the surface but also along the k_z direction with relatively high bulk sensitivity [39,40]. A renormalized band was successfully observed along a specific direction in reciprocal space, which was not seen in the ARPES spectra of the non-$4f$ system $LaNi_2Ge_2$ with almost equivalent experimental conditions to those for $CeNi_2Ge_2$. Moreover, a direct comparison with $LaNi_2Ge_2$, which is a non-$4f$ system with $\gamma = 14.5$ mJ/(mol K^2) [41], gives quantitative evidence of the mass enhancement in $CeNi_2Ge_2$ from $LaNi_2Ge_2$.

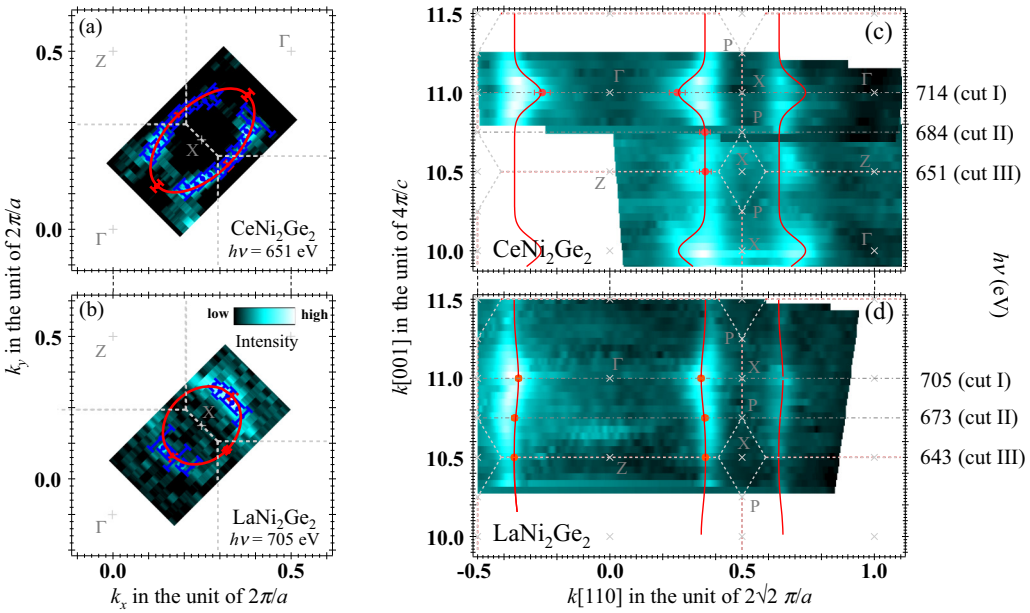

FIG. 1. FS slices in the (a), (b) k_x-k_y and (c), (d) k_{xy}-k_z planes of $CeNi_2Ge_2$ and $LaNi_2Ge_2$, which are obtained by integrating the photoelectron intensity between the Fermi level and unoccupied −0.2 eV. The dashed lines represent the BZ boundaries. The dots with error bars represent the k_F's estimated from each specific angle slice. The solid lines are guides to the eye of Fermi surfaces following the experimentally evaluated k_F's. The dashed-dotted lines of (c) and (d) indicate incident photon energies.

II. EXPERIMENT

High-quality RNi_2Ge_2 (R = Ce, La) single crystals were grown by the Czochralski method [42]. The ARPES experiments were performed at the twin helical undulator beamline BL23SU of SPring-8 [43]. The ARPES spectra were acquired using a Gammadata-Scienta SES-2002 electron analyzer. The energy resolution was set to about 70–130 meV for a photon energy ($h\nu$) of about 580–780 eV for the angle-resolved experiments. The sample temperature was set to 10 K (Fig. 1)

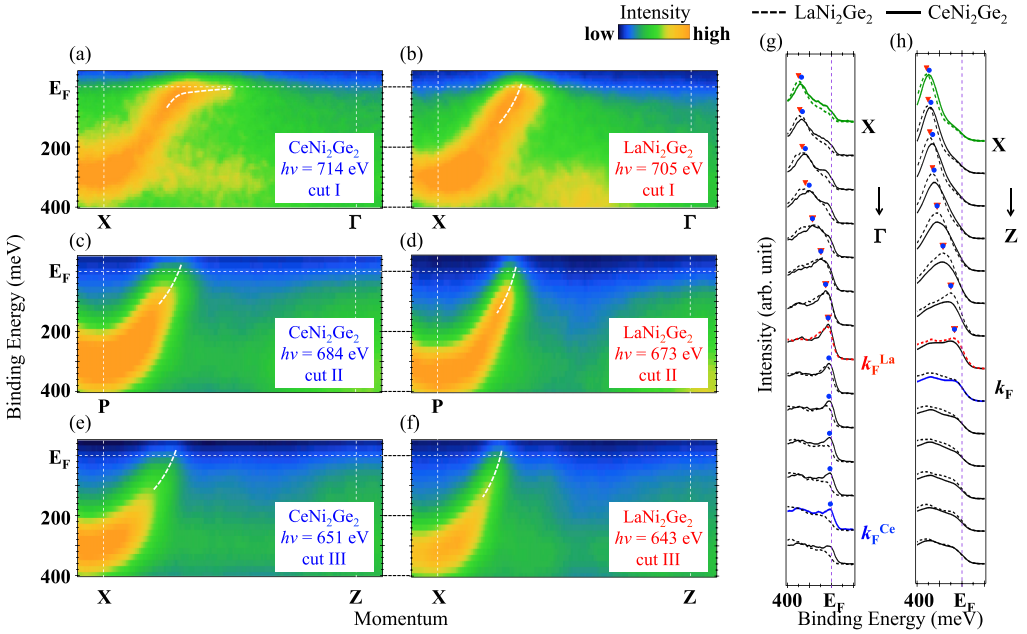

FIG. 2. (a)–(f) ARPES intensity plots of RNi_2Ge_2 (R = Ce, La) along cut I ($k_z = 0$, Γ-X), cut II ($k_z = \pi/c$), and cut III ($k_z = 2\pi/c$, Z-X). The energy resolution of the data in (a) and (b) was set to 70 meV, and that in (c)–(f) was set to 130 meV while the sample temperature was set to 8 K. The curved dashed lines represent guides to the eye. (g), (h) Energy distribution curves of $CeNi_2Ge_2$ (solid lines) and $LaNi_2Ge_2$ (dashed lines) along the (g) Γ-X and (h) Z-X directions. The labels k_F^{La} and k_F^{Ce} in (g) represent the Fermi momentum of $LaNi_2Ge_2$ and $CeNi_2Ge_2$ along the Γ-X direction, respectively. The label k_F in (h) represents the Fermi momentum of both compounds. The peak positions corresponding to the band structure are indicated by circles for $CeNi_2Ge_2$ and triangles for $LaNi_2Ge_2$.

and 8 K (Fig. 2), which is low enough to have a better chance of accessing HF states [12]. The single-crystal samples were cleaved in a base pressure of about 8.8×10^{-9} Pa to expose clean (001) surfaces. The sample qualities were examined on the basis of the absence of O and C 1s core-level peaks caused by possible impurities or surface oxidization [44].

III. RESULTS AND DISCUSSION

Figure 1 shows an evolution of the Fermi surface (FS) from $LaNi_2Ge_2$ to $CeNi_2Ge_2$ obtained by $h\nu$-dependent ARPES, which has an advantage of clarifying the bulk FS topology in the 3D Brillouin zone (BZ) [17]. The FS topology in the k_x-k_y plane is circular for $LaNi_2Ge_2$, as shown in Fig. 1(b), but that for $CeNi_2Ge_2$ in Fig. 1(a) is elliptical with the major axis along the Γ-X line. A difference in shape between $LaNi_2Ge_2$ and $CeNi_2Ge_2$ is also observed in the k_z mapping. The FS of $LaNi_2Ge_2$ only weakly depends on k_z having a quasi-two-dimensional shape, as indicated by the solid lines in Fig. 1(d). This contrasts sharply with the FS of $CeNi_2Ge_2$, which shows a strong k_z dependence around the X points in Fig. 1(c).

This change is related to the increase in the $4f$ electron number from La to Ce as discussed below, and thus significant $4f$ electron contributions to the band dispersion are expected in the Γ-X direction, labeled as cut I in Fig. 1 with $k_z = 11.0$ in units of $4\pi/c$, where c stands for the out-of-plane lattice constant of $CeNi_2Ge_2$ with a body-centered-tetragonal structure. Note that the resonance ARPES at the Ce $4d$-$4f$ and $3d$-$4f$ edges cannot access the Γ-X direction because of a corresponding k_z of 4.6 [equivalent to 10.6 in Fig. 1(a), between cuts II and III] and 12.23 (equivalent to 10.77, cut II), respectively.

Detailed k_z-dependent band dispersions are displayed in Figs. 2(a)–2(f), which show intensity plots along cuts I, II, and III. In Fig. 2(a), the band of $CeNi_2Ge_2$ becomes flat upon approaching E_F, in contrast to the simple parabolic band of $LaNi_2Ge_2$ in Fig. 2(b). This gives direct evidence of the formation of the HF electronic structure in $CeNi_2Ge_2$ that the itinerant conduction band hybridizes with the localized $4f$ orbitals [45]. Such HF behavior is not observed in cuts II and III, in which a paraboliclike shape comparable to that of $LaNi_2Ge_2$ is observed, as shown in Figs. 2(c)–2(f). This indicates that the heavy fermionic electronic structure is present at only a specific momentum along the Γ-X cut. Note that the flatband at 300 meV as shown in Fig. 2(a) is not due to the Ce $4f$ states since it is also observed for $LaNi_2Ge_2$ with nominally no $4f$ occupation, as shown in Fig. 2(b) [46].

The detailed differences in the electronic structure are given by a comparison of the energy distribution curves (EDCs) shown in Figs. 2(g) and 2(h). The spectral weights in the vicinity of E_F along the Γ-X direction from k_F^{La} (0.33 Å^{-1}) to k_F^{Ce} (0.52 Å^{-1}) [47] (hereafter referred to as a "heavy spot") of $CeNi_2Ge_2$ displayed in Fig. 2(g) are large and still maintain the peak structures compared to those of $LaNi_2Ge_2$, indicating a larger Fermi surface of $CeNi_2Ge_2$. This behavior is consistent with the enlargement of the FS from $LaNi_2Ge_2$ to $CeNi_2Ge_2$ along the Γ-X cut in Fig. 1. On the other hand, the peak positions of both compounds in EDCs along the Z-X direction in Fig. 2(h) are comparable and the peaks disappear around the equivalent momentum. Moreover, the energies of the band bottom are almost identical for both Ce and La systems, and thus the simple rigid band model caused by the increase in the electron number from La to Ce atom is ruled out. Therefore, we stress that the anisotropic enlargement of the FS along the Γ-X direction indicates momentum-dependent HF behavior, which is not predicted from density functional theories [42,48].

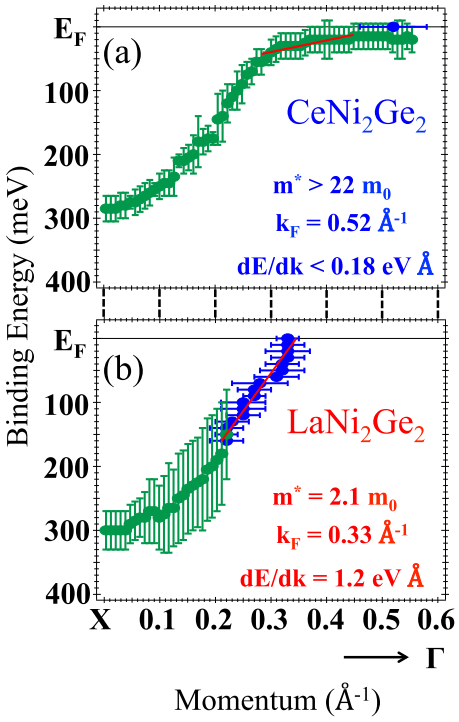

FIG. 3. Obtained band dispersion near E_F of (a) $CeNi_2Ge_2$ and (b) $LaNi_2Ge_2$ along the Γ-X direction from the peak binding positions of energy distribution curves (with error bars along energy) and momentum distribution curves (with error bars along momentum). The straight lines represent the estimated band slopes.

The effective mass of the observed bands of RNi_2Ge_2 (R = Ce, La) is estimated from the peak binding energies in Figs. 2(g) and 2(h), using formulas (1) and (2). The peak positions of EDCs and momentum distribution curves (MDCs) along the Γ-X directions are plotted in Figs. 3(a) and 3(b). The band slope of $LaNi_2Ge_2$ is estimated by the straight line in the figure, which is determined by a least-square fit to the data. The effective mass of $LaNi_2Ge_2$ along the Γ-X line is $m^*_{La} = 2.1m_0$ (m_0 is the free electron mass), which is consistent with the results of a de Haas–van Alphen (dHvA) experiment [49] and of the *ab initio* calculations with an all-electron fully relativistic augmented-plane-wave method [48].

In estimating the effective mass of $CeNi_2Ge_2$ along the Γ-X cut, we have used the peak energies of EDCs because the peak momenta of MDCs do not simply represent the quasiparticle dispersions due to the drastic change in the non-$4f$ contributions in the spectra as a function of momentum between k_F^{La} and k_F^{Ce}, which originates from cf-hybridization effects. The MDC analysis can be effective when the orbital character does not depend on momentum (Appendix A). Since it is difficult to precisely estimate the effective mass, relatively large $|dE/dk|_{k=k_F}$ are estimated, as shown in Fig. 3(a), to determine the lower limit of the effective mass, which enables

TABLE I. The effective mass of RNi$_2$Ge$_2$ (R = Ce, La) along three directions measured in this study.

Line	$LaNi_2Ge_2$	$CeNi_2Ge_2$
$k_z = 0$	$(2.1 \pm 0.4)m_0$	$> 22m_0$
$k_z = \pi/c$	$(0.6 \pm 0.4)m_0$	$(1.2 \pm 0.8)m_0$
$k_z = 2\pi/c$	$(0.9 \pm 0.5)m_0$	$(1.5 \pm 0.6)m_0$

us to avoid an overestimation of the effective mass. The band mass of $CeNi_2Ge_2$ along the Γ-X line is $m^*_{Ce} > 22m_0$, which corresponds to a mass enhancement factor of $m^*_{Ce}/m^*_{La} > 10$. According to the periodic Anderson model which reasonably reproduces the experimental dispersion (Appendix B), the m^*_{Ce}/m^*_{La} is evaluated as 66. We have also estimated the band mass of both compounds along the other directions, as summarized in Table I (see also Appendix C). A 24 times larger Sommerfeld coefficient [3,41] would be reasonable when we consider a mass enhancement factor of $m^*_{Ce}/m^*_{La} = 66$ along the Γ-X line and a heavy ($m^*_{Ce}/m^*_{La} \gg 2$) fermionic electronic structure is not observed in the other directions.

Our results of the estimated k_F^{Ce} of 0.52 Å^{-1} correspond to 50% of the Γ-X period for $CeNi_2Ge_2$ in the k_x-k_y plane, as shown in Fig. 4. According to the neutron scattering measurement [50], on the other hand, an antiferromagnetic correlation modulated by a wave vector $(\frac{1}{2}\frac{1}{2}0)$ has been detected in $CeNi_2Ge_2$. Therefore, the wave vectors between the heavy spots in the (001) plane correspond well to the antiferromagnetic wave vector in Fig. 4. The states in the vicinity of k_F^{Ce} with a heavy mass are effectively enhanced, which leads to a large energy gain of the Cooper-pair formation in the superconducting phase. Thus, the spin fluctuation, which is

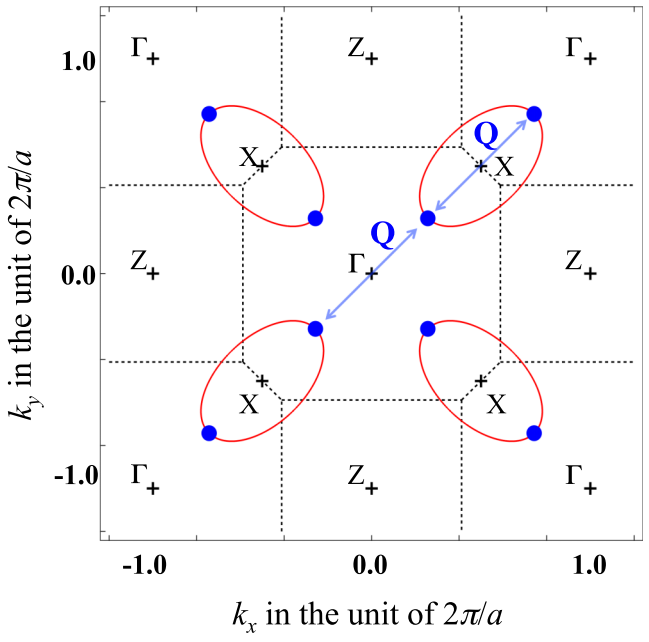

FIG. 4. Schematic drawing of FS of $CeNi_2Ge_2$ together with the BZ, where a denotes the lattice constant. The dots represent the observed HF k_Fs. The arrows represent the wave vectors between k_F's in the (001) plane of HF electronic structure.

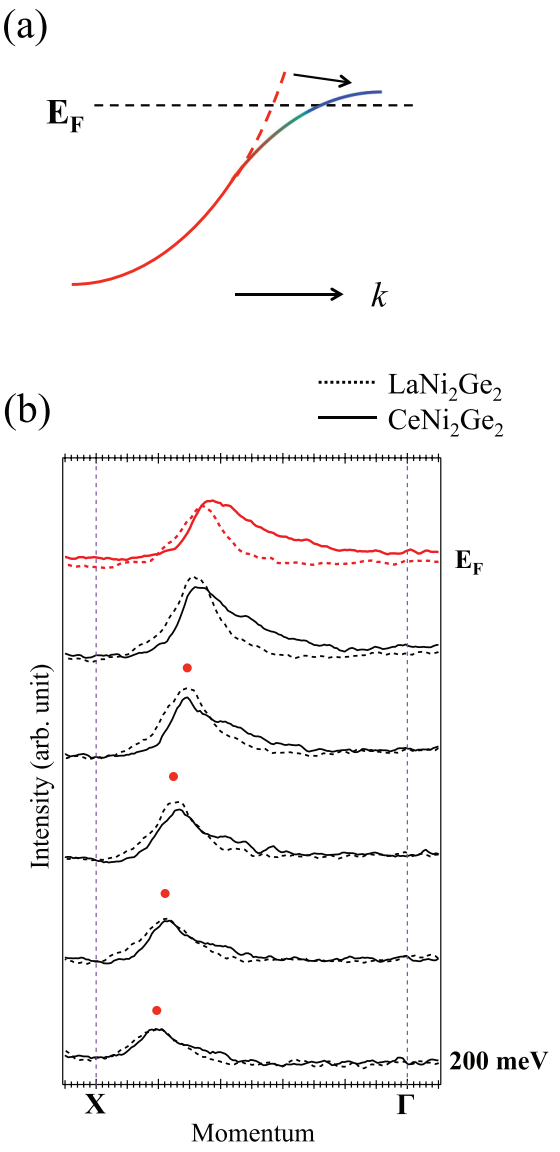

FIG. 5. (a) Schematic drawing of the electronic structure in the presence of cf hybridization. (b) Momentum distribution curves of $CeNi_2Ge_2$ (solid line) and $LaNi_2Ge_2$ (dashed line) along the Γ-X direction.

proposed in several theories [25–27], should play an important role in the superconductivity in $CeNi_2Ge_2$. The importance of the spin fluctuation scenario is also confirmed by volume thermal expansion and specific heat measurements [51]. Our results propose the importance of detecting heavy spots for the origin of quantum critical phenomena in heavy fermion compounds.

IV. CONCLUSION

In conclusion, we have succeeded in observing clear experimental evidence of an anisotropic large Fermi surface and the momentum-dependent heavy fermionic electronic structure of $CeNi_2Ge_2$ by soft x-ray ARPES. This study provides a promising approach to HF states; we should select the momentum for the observation of HF states. The detected

wave vectors of the heavy spots seem to be related to the magnetic correlations, as discussed in high-T_c superconducting cuprates [52].

ACKNOWLEDGMENTS

We acknowledge the help and support of Y. Takeda of JAEA during the beam time. We also thank H. Fuchimoto, S. Naimen, Y. Nakata, K. Takeuchi, D. Iwasaki, Y. Higashino, C. Yoshimi, T. Yagi, Y. Kanai, Y. Nakamura, W. Zhu, and T. Hirano for supporting the measurements. The measurements were performed under the approval of BL23SU at SPring-8 (Proposals No. 2013B3882 and No. 2014B3882). This work was supported by a Grant-in-Aid for Scientific Research (16H04014), and a Grant-in-Aid for Innovative Areas (20102003 and 16H01074) from MEXT and JSPS, Japan. Y.N. was supported by the Program for Leading Graduate Schools Interactive Materials Science Cadet Program and JSPS Research Fellowships for Young Scientists.

APPENDIX A: MOMENTUM DISTRIBUTION CURVES ALONG THE Γ-X DIRECTION

Figure 5 shows the MDCs of $CeNi_2Ge_2$ and $LaNi_2Ge_2$ along the Γ-X direction, together with a schematic drawing of the electronic structure in the presence of cf hybridization. Although the peak positions of $CeNi_2Ge_2$ are close to those of $LaNi_2Ge_2$, as indicated by the circles in Fig. 5(b), the MDC of $CeNi_2Ge_2$ at E_F is asymmetric and has a stronger intensity towards the Γ point than that of $LaNi_2Ge_2$. The observed asymmetry reflects a drastic change in the band structure, as illustrated in Fig. 5(a). Generally, the orbital character of a cf-hybridized band depends on momentum; it changes from non-4f to 4f contributions with approaching E_F. Since the photoionization cross section for the Ce 4f state is smaller than the other orbitals in the valence band of $CeNi_2Ge_2$ [53], the photoelectron intensity should be small with approaching E_F. Although the peak positions of MDCs do not simply represent the hybridized band dispersion, the asymmetry of MDC implies a heavy fermion state.

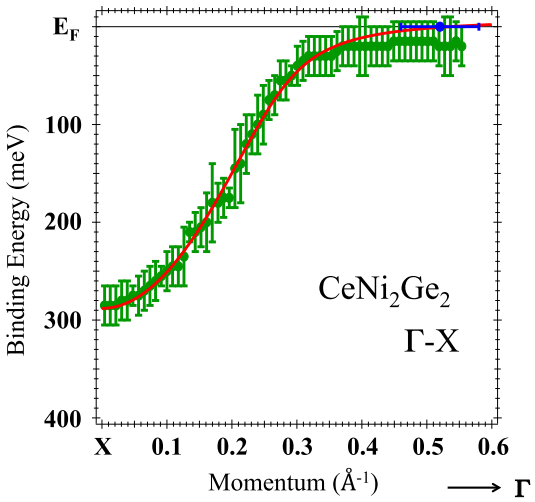

FIG. 6. Comparison of the best simulated cf-hybridized dispersion by the periodic Anderson model (solid curve) giving $m^*_{Ce}/m^*_{La} = 66$ with the experimentally obtained band dispersion (circles with error bars) of $CeNi_2Ge_2$ along the Γ-X cut as shown in Fig. 3(a).

APPENDIX B: PERIODIC ANDERSON MODEL

Figure 6 shows a comparison between the result of ARPES and the theoretical calculation. The calculation is based on a periodic Anderson model with the use of the leading order of $1/N$ expansion [54,55].

With the use of pseudoparticles, the infinite-U periodic Anderson model is given by

$$H = \sum_{m=1}^{N}\sum_{\boldsymbol{k}_m}\epsilon^{(0)}_{\boldsymbol{k}_m} c^{+}_{m\boldsymbol{k}_m} c_{m\boldsymbol{k}_m} + \sum_{i=1}^{N_L}\sum_{m=1}^{N}\epsilon^{(0)}_{f} f^{+}_{mi} f_{mi} + \frac{1}{\sqrt{N_L}}\sum_{mi\boldsymbol{k}_m}(V_{k_m} e^{-i\boldsymbol{k}_m \boldsymbol{R}_i} c^{+}_{m\boldsymbol{k}_m} f_{mi} b^{+}_{i} + \text{H.c.}), \quad \text{(B1)}$$

where m denotes the component of the spin-orbital degeneracy $N = 2$ of the Γ_7 states in the crystalline electric field scheme of $CeNi_2Ge_2$[56] in an f^1 configuration; $c_{m\boldsymbol{k}_m}$, f_{mi}, and b_i represent the annihilation operator of a conduction electron with wave vector $\boldsymbol{k}_m$, spin-orbital component m, the pseudofermion representing the f^1 state with m at the i site, and the slave boson representing f^0 state at the i site; V_{k_m} represents the hybridization transforming from the f^1 state to the conduction electron; and N_L is the total number of lattice sites. To guarantee a physical equivalence between the present model and the original $U = \infty$ model, this Hamiltonian must be treated within the subspace where the local constraint,

$$Q_i = \sum_m f^{+}_{mi} f_{mi} + b^{+}_{i} b_i, \quad \text{(B2)}$$

holds.

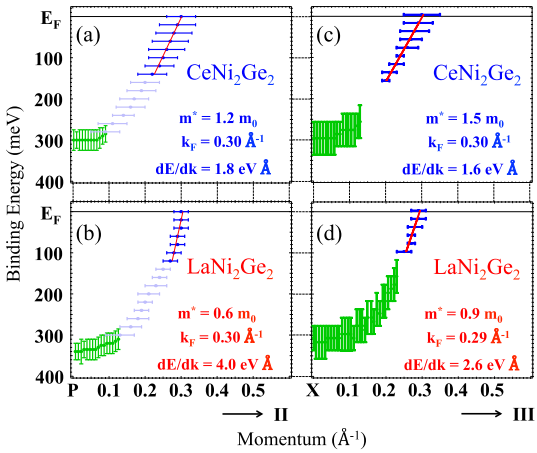

FIG. 7. Obtained band dispersion near E_F for RNi_2Ge_2 (R = Ce, La) along cut II ($k_z = \pi/c$) and cut III ($k_z = 2\pi/c$, Z-X) from the peak positions of the energy distribution curves (with error bars along energy) and momentum distribution curves (with error bars along momentum). The straight line represents the estimated band slope.

We use the perturbational expansion in powers of $1/N$. By including terms on the order of $(1/N)^0$, the Green's function for the conduction electron $G_{\boldsymbol{k}_m}(z)$ is given by

$$G_{\boldsymbol{k}_m}(z) = \frac{1}{z - \epsilon_{\boldsymbol{k}_m} - \frac{a|V_{\boldsymbol{k}_m}|^2}{z - E_0}}, \tag{B3}$$

where $\epsilon_{\boldsymbol{k}_m} = \epsilon^{(0)}_{\boldsymbol{k}_m} - \mu$, $\epsilon_f = \epsilon^{(0)}_f - \mu$, where μ is the chemical potential, E_0 is the binding energy of the slave boson and corresponds to the Kondo temperature $T_{\rm K} = D\exp(-1/|J|N_F)$ in the impurity Anderson model, where D is the half width of the band for the conduction electrons, J is the cf-exchange interaction, and $N_{\rm F}$ is the density of states of the conduction electrons, and a is the residue of the slave boson and corresponds to $T_{\rm K}/\pi N_{\rm F}|V_{\boldsymbol{k}_m}|^2$ in the impurity Anderson model. E_0 and a are determined by solving the following coupled equations,

$$\epsilon_f - E_0 - \frac{1}{N_L}\sum_{m\boldsymbol{k}_m}|V_{\boldsymbol{k}_m}|^2 \int d\epsilon f(\epsilon)\frac{-1}{\pi} \times \mathrm{Im}\, G_{m\boldsymbol{k}_m}(\epsilon + i0_+)\frac{1}{\epsilon - E_0} = 0, \tag{B4}$$

$$\frac{1}{a} = 1 + \frac{1}{N_L}\sum_{m\boldsymbol{k}_m}|V_{\boldsymbol{k}_m}|^2 \int d\epsilon f(\epsilon)\frac{-1}{\pi} \times \mathrm{Im}\, G_{m\boldsymbol{k}_m}(\epsilon + i0_+)\frac{1}{(\epsilon - E_0)^2}. \tag{B5}$$

To reproduce the result of ARPES along the Γ-X direction, we use $\epsilon^{(0)}_{\boldsymbol{k}} = -D\cos(ka)$, and we choose the parameters $D = 1$, $\epsilon^{(0)}_f = -0.77$, $V_{\boldsymbol{k}_m} = 0.13$, and $\mu = -0.722$, which lead to $E_0 = 1.11 \times 10^{-2}$ in units of the bandwidth, $a = 0.475$ in units of Γ-X distance, and the mass enhancement factor $m^*_{\rm Ce}/m^*_{\rm La} = 66$.

APPENDIX C: ESTIMATION OF THE EFFECTIVE MASSES FOR CUTS II AND III

Figure 7 displays the peak positions of EDCs and MDCs along cuts II and III. The effective masses of these cuts are estimated by the peak positions of MDCs. The least-square fitting was employed by assuming a linearly dispersive band to obtain the band slope. The estimated effective masses along each direction are summarized in Table I.

[1] K. Andres and J. E. Graebner, Phys. Rev. Lett. **35**, 1779 (1975).
[2] F. Steglich, J. Aarts, C. D. Bredl, W. Lieke, D. Meschede, W. Franz, and H. Schäfer, Phys. Rev. Lett. **43**, 1892 (1979).
[3] F. Steglich, B. Buschinger, P. Gegenwart, M. Lohmann, R. Helfrich, C. Langhammer, P. Hellmann, L. Donnevert, S. Thomas, A. Link, C. Geibel, M. Lang, G. Sparn, and W. Assmus, J. Phys.: Condens. Matter **8**, 9909 (1996).
[4] M. J. Besnus, J. P. Kappler, P. Lehmann, and A. Meyer, Solid State Commun. **55**, 779 (1985).
[5] F. M. Grosche, P. Agarwal, S. R. Julian, N. J. Wilson, R. K. W. Haselwimmer, S. J. S. Lister, N. D. Mathur, F. V. Carter, S. S. Saxena, and G. G. Lonzarich, J. Phys.: Condens. Matter **12**, L533 (2000).
[6] F. R. de Boer, J. C. P. Klaasse, P. A. Veenhuizen, A. Bohm, C. D. Bredl, U. Gottwick, H. M. Mayer, L. Pawlak, U. Rauchschwalbe, H. Spille, and F. Steglich, J. Magn. Magn. Mater. **63–64**, 91 (1987).
[7] D. Jaccard, K. Behnia, and J. Sierro, Phys. Lett. A **163**, 475 (1992).
[8] H. Hegger, C. Petrovic, E. G. Moshopoulou, M. F. Hundley, J. L. Sarrao, Z. Fisk, and J. D. Thompson, Phys. Rev. Lett. **84**, 4986 (2000).
[9] G. Knebel, D. Braithwaite, P. C. Canfield, G. Lapertot, and J. Flouquet, Phys. Rev. B **65**, 024425 (2001).
[10] M. Yashima, S. Kawasaki, H. Mukuda, Y. Kitaoka, H. Shishido, R. Settai, and Y. Ōnuki, Phys. Rev. B **76**, 020509 (2007).
[11] J. D. Denlinger, G.-H. Gweon, J. W. Allen, C. G. Olson, M. B. Maple, J. L. Sarrao, P. E. Armstrong, Z. Fisk, and H. Yamagami, J. Electron Spectrosc. Relat. Phenom. **117–118**, 347 (2001).
[12] A. Koitzsch, S. V. Borisenko, D. Inosov, J. Geck, V. B. Zabolotnyy, H. Shiozawa, M. Knupfer, J. Fink, B. Büchner, E. D. Bauer, J. L. Sarrao, and R. Follath, Phys. Rev. B **77**, 155128 (2008).
[13] H. J. Im, T. Ito, H.-D. Kim, S. Kimura, K. E. Lee, J. B. Hong, Y. S. Kwon, A. Yasui, and H. Yamagami, Phys. Rev. Lett. **100**, 176402 (2008).
[14] T. Ohkochi, T. Toshimitsu, Hiroshi Yamagami, S.-i. Fujimori, A. Yasui, Y. Takeda, T. Okane, Y. Saitoh, A. Fujimori, Y. Miyauchi, Y. Okuda, R. Settai, and Y. Ōnuki, J. Phys. Soc. Jpn. **78**, 084802 (2009).
[15] T. Okane, T. Ohkochi, Y. Takeda, S.-i. Fujimori, A. Yasui, Y. Saitoh, H. Yamagami, A. Fujimori, Y. Matsumoto, M. Sugi, N. Kimura, T. Komatsubara, and H. Aoki, Phys. Rev. Lett. **102**, 216401 (2009).
[16] T. Okane, T. Ohkochi, Y. Takeda, S.-i. Fujimori, A. Yasui, Y. Saitoh, H. Yamagami, A. Fujimori, Y. Matsumoto, M. Sugi, N. Kimura, T. Komatsubara, and H. Aoki, Phys. Status Solidi B **247**, 697 (2010).
[17] M. Yano, A. Sekiyama, H. Fujiwara, T. Saita, S. Imada, T. Muro, Y. Ōnuki, and S. Suga, Phys. Rev. Lett. **98**, 036405 (2007).
[18] M. Yano, A. Sekiyama, H. Fujiwara, Y. Amano, S. Imada, T. Muro, M. Yabashi, K. Tamasaku, A. Higashiya, T. Ishikawa, Y. Ōnuki, and S. Suga, Phys. Rev. B **77**, 035118 (2008).
[19] D. V. Vyalikh, S. Danzenbächer, Yu. Kucherenko, C. Krellner, C. Geibel, C. Laubschat, M. Shi, L. Patthey, R. Follath, and S. L. Molodtsov, Phys. Rev. Lett. **103**, 137601 (2009).
[20] D. V. Vyalikh, S. Danzenbächer, Yu. Kucherenko, K. Kummer, C. Krellner, C. Geibel, M. G. Holder, T. K. Kim, C. Laubschat, M. Shi, L. Patthey, R. Follath, and S. L. Molodtsov, Phys. Rev. Lett. **105**, 237601 (2010).
[21] A. Koitzsch, T. K. Kim, U. Treske, M. Knupfer, B. Büchner, M. Richter, I. Opahle, R. Follath, E. D. Bauer, and J. L. Sarrao, Phys. Rev. B **88**, 035124 (2013).
[22] M. Y. Kimura, K. Fukushima, H. Takeuchi, S. Ikeda, H. Sugiyama, Y. Tomida, G. Kuwahara, H. Fujiwara, T. Kiss, A. Yasui, I. Kawasaki, H. Yamagami, Y. Saitoh, T. Muro, T. Ebihara, and A. Sekiyama, J. Phys.: Conf. Ser. **592**, 012003 (2015).

[23] Y. Zhang, H. Lu, X. Zhu, S. Tan, Q. Liu, Q. Chen, W. Feng, D. Xie, L. Luo, Y. Liu, H. Song, Z. Zhang, and X. Lai, Sci. Rep. **6**, 33613 (2016).
[24] S. Patil, A. Generalov, M. Güttler, P. Kushwaha, A. Chikina, K. Kummer, T. C. Rödel, A. F. Santander-Syro, N. Caroca-Canales, C. Geibel, S. Danzenbächer, Yu. Kucherenko, C. Laubschat, J. W. Allen, and D. V. Vyalikh, Nat. Commun. **7**, 11029 (2017).
[25] T. Moriya and A. Kawabata, J. Phys. Soc. Jpn. **34**, 639 (1973); **35**, 669 (1973).
[26] Q. Si, S. Rabello, K. Ingersent, and J. L. Smith, Nature (London) **413**, 804 (2001).
[27] P. Coleman, C. Pépin, Q. Si, and R. Ramazashvili, J. Phys.: Condens. Matter **13**, R723 (2001).
[28] Q. Si and F. Steglich, Science **329**, 1161 (2010).
[29] S. Watanabe and K. Miyake, Phys. Rev. Lett. **105**, 186403 (2010).
[30] S. Watanabe and K. Miyake, J. Phys.: Condens. Matter **23**, 094217 (2011); **24**, 294208 (2012).
[31] P. Hansmann, A. Severing, Z. Hu, M. W. Haverkort, C. F. Chang, S. Klein, A. Tanaka, H. H. Hsieh, H.-J. Lin, C. T. Chen, B. Fåk, P. Lejay, and L. H. Tjeng, Phys. Rev. Lett. **100**, 066405 (2008).
[32] T. Willers, D. T. Adroja, B. D. Rainford, Z. Hu, N. Hollmann, P. O. Körner, Y.-Y. Chin, D. Schmitz, H. H. Hsieh, H.-J. Lin, C. T. Chen, E. D. Bauer, J. L. Sarrao, K. J. McClellan, D. Byler, C. Geibel, F. Steglich, H. Aoki, P. Lejay, A. Tanaka, L. H. Tjeng, and A. Severing, Phys. Rev. B **85**, 035117 (2012).
[33] Y. Saitoh, H. Fujiwara, T. Yamaguchi, Y. Nakatani, T. Mori, H. Fuchimoto, T. Kiss, A. Yasui, J. Miyawaki, S. Imada, H. Yamagami, T. Ebihara, and A. Sekiyama, J. Phys. Soc. Jpn. **85**, 114713 (2016).
[34] J. Stöhr, J. Electron Spectrosc. Relat. Phenom. **75**, 253 (1995).
[35] B. T. Thole, G. van der Laan, J. C. Fuggle, G. A. Sawatzky, R. C. Karnatak, and J.-M. Esteva, Phys. Rev. B **32**, 5107 (1985).
[36] J. B. Goedkoop, B. T. Thole, G. van der Laan, G. A. Sawatzky, F. M. F. de Groot, and J. C. Fuggle, Phys. Rev. B **37**, 2086 (1988).
[37] J. C. Fuggle, F. U. Hillebrecht, J.-M. Esteva, R. C. Karnatak, O. Gunnarsson, and K. Schönhammer, Phys. Rev. B **27**, 4637 (1983).
[38] See Supplemental Material at http://link.aps.org/supplemental/10.1103/PhysRevB.97.115160 for the satellite intensity reflecting the cf hybridization.
[39] A. Sekiyama, T. Iwasaki, K. Matsuda, Y. Saitoh, Y. Ōnuki, and S. Suga, Nature (London) **403**, 396 (2000).
[40] S. Tanuma, C. J. Powell, and D. R. Penn, Surf. Interface Anal. **43**, 689 (2011).
[41] S. Kasahara, H. Fujii, H. Takeya, T. Mochiku, A. D. Thakur, and K. Hirata, J. Phys.: Condens. Matter **20**, 385204 (2008).
[42] D. Ehm, F. Reinert, G. Nicolay, S. Schmidt, S. Hüfner, R. Claessen, V. Eyert, and C. Geibel, Phys. Rev. B **64**, 235104 (2001).
[43] Y. Saitoh, Y. Fukuda, Y. Takeda, H. Yamagami, S. Takahashi, Y. Asano, T. Hara, K. Shirasawa, M. Takeuchi, T. Tanaka, and H. Kitamura, J. Synchrotron Radiat. **19**, 388 (2012).
[44] The absence of O and C 1s peaks in the core-level photoemission spectrum can be found in the Supplemental Material [38].
[45] The HF behavior can also be confirmed by the ARPES spectra with a relatively poor resolution, as shown in the Supplemental Material [38].
[46] Y. Nakatani, H. Fujiwara, H. Aratani, T. Mori, S. Tachibana, T. Yamaguchi, T. Kiss, A. Yamasaki, A. Yasui, H. Yamagami, A. Tsuruta, J. Miyawaki, T. Ebihara, Y. Saitoh, and A. Sekiyama, J. Electron Spectrosc. Relat. Phenom. **220**, 50 (2017).
[47] Detailed information on how to determine the Fermi momentum is given in the Supplemental Material [38].
[48] H. Yamagami, J. Phys. Soc. Jpn. **68**, 1975 (1999).
[49] K. Maezawa, S. Sakane, T. Fukuhara, H. Ohkuni, R. Settai, and Y. Ōnuki, Physica B **259–261**, 1091 (1999).
[50] H. Kadowaki, B. Fåk, T. Fukuhara, K. Maezawa, K. Nakajima, M. A. Adams, S. Raymond, and J. Flouquet, Phys. Rev. B **68**, 140402 (2003).
[51] R. Küchler, N. Oeschler, P. Gegenwart, T. Cichorek, K. Neumaier, O. Tegus, C. Geibel, J. A. Mydosh, F. Steglich, L. Zhu, and Q. Si, Phys. Rev. Lett. **91**, 066405 (2003).
[52] A. Damascelli, Z. Hussain, and Z.-X. Shen, Rev. Mod. Phys. **75**, 473 (2003).
[53] J. J. Yeh and I. Lindau, At. Data Nucl. Data Tables **32**, 1 (1985).
[54] Y. Ono, T. Matsuura, and Y. Kuroda, Physica C **159**, 878 (1989).
[55] A. Tsuruta, A. Kobayashi, T. Matsuura, and Y. Kuroda, J. Phys. Soc. Jpn. **69**, 3342 (2000).
[56] Y. Aoki, J. Urakawa, H. Sugawara, H. Sato, T. Fukuhara, and K. Maezawa, J. Phys. Soc. Jpn. **66**, 2993 (1997).